

Channel Estimation in TDD Cell-free Scenario using OTFS Modulation

Yatish Pachigolla, Lorenzo Zaniboni, Mahdi Mahvari

Technical University of Munich, Germany

Emails: {yatish.pachigolla, lorenzo.zaniboni, mahdi.mahvari}@tum.de

Abstract—Channel estimation techniques for orthogonal time frequency space (OTFS) modulation scheme are investigated. The orthogonal matching pursuit algorithm is investigated with and without side channel information and an efficient data placement is proposed alongside the pilot in the multi-user scenario based on impulse pilot-based estimation. Finally, the algorithms are compared in different multi-user scenarios with numerical results.

Index Terms—Orthogonal Time Frequency Space Modulation, Orthogonal Matching Pursuit, Channel Estimation

I. INTRODUCTION

Massive multiple-input multiple-output (MIMO) technology combines high data rates with efficient processing [1]. For a large geographic region, one generally uses distributed antenna structures, called access points (APs), connected by backhaul links [2]. The distributed structure provides macro-diversity gain by allowing a large number of APs to communicate with a relatively smaller number of user equipments (UEs), unlike traditional massive MIMO where each UE is served by a single base station. The system has no cell boundaries and is called cell-free massive MIMO [3]. The APs are often assumed to be single antenna devices that serve users in a time-division duplex (TDD) mode. Future networks may need advanced modulation schemes to support time and frequency-varying channels, also called doubly-selective channels. Orthogonal time frequency space (OTFS) modulation [4], [5] can provide higher data rates than orthogonal frequency-division multiplexing (OFDM) in scenarios with high Doppler shifts [6]–[10]. OTFS can be considered as a precoded OFDM where the information symbols are placed in the delay-Doppler (DD) domain. The information symbols are transformed to the time-frequency (TF) domain through the Zak transform and are sent to the receiver with OFDM modulation [11], [12].

One challenge in cell-free massive MIMO systems is accurate channel estimation [13], [14]. As users are served by multiple distributed APs, the channel state information (CSI) becomes complex due to more diverse interference and channel characteristics. The paper [15] estimates the delay, Doppler, and channel gains using pseudo-noise (PN) sequences as pilots. This method has large complexity because it estimates the delay-Doppler coefficients in the TF domain. The paper [16] has each antenna transmit a single pilot impulse in a frame to estimate the channel. This leads to a large loss in spectral efficiency because most frames containing the pilot

cannot carry data. Moreover, this method may generate errors in estimation when applied to rapidly time-varying channels because the channel information estimated by the pilot in each frame is utilized for data detection in the subsequent frame. Accordingly, [17] places multiple pilot impulses in a single frame with sufficient guard bands depending on the maximum delay and Doppler spreads associated with the channel.

An important aspect of OTFS modulation is that it has a sparse DD channel representation [5]. This sparsity is utilized by a variety of algorithms. For example, the papers [18], [19] propose a sparse Bayesian learning method, [20] improved the complexity of approximate message passing (AMP), and [21] uses orthogonal matching pursuit (OMP) for multiple users. To further improve the spectral efficiency, the paper [22] introduced an embedded pilot-aided channel estimation, where the data and pilot symbols are placed in the same frame. Similarly, [23] placed both data and pilot symbols in the same frame with different power levels.

The main contributions of this paper are as follows:

- a comparison of OMP and threshold-based channel estimation for different multi-user scenarios;
- a study of OMP-based channel estimation with side channel information (SCI);
- a bandwidth-efficient pilot and data placement for multi-user channel estimation and data detection.

Notation: We use the following notation. $(\cdot)^*$, $(\cdot)^\top$, and $(\cdot)^H$ denote the complex conjugate, transpose, and Hermitian (conjugate and transpose) operations, respectively. $|x|$ is the absolute value of $x \in \mathbb{R}$ and $|\mathcal{X}|$ denotes the cardinality of the set \mathcal{X} . $\|\mathbf{x}\|_p$ is the ℓ_p -norm of a complex or real vector \mathbf{x} . \mathbf{F}_D is the D dimensional discrete Fourier transform (DFT) matrix. The $m \times m$ identity matrix is written as \mathbf{I}_m , we write $[n] = \{0, 1, \dots, n-1\}$.

II. SYSTEM MODEL

Consider an AP and UEs $u \in \{1, \dots, U\}$ that communicate over a sparse channel

$$h_u(\tau, \nu) = \sum_{i=0}^{L-1} h_{i,u} \delta(\tau - \tau_{i,u}) \delta(\nu - \nu_{i,u}) \quad (1)$$

in the DD domain, where L is the number of paths. $h_{i,u}$, $\tau_{i,u}$, and $\nu_{i,u}$ are the channel coefficient, delay, and Doppler shift

associated with the i -th path and the user u , respectively. The delay and Doppler taps associated with the i -th path are

$$\tau_{i,u} = \frac{l_{i,u}}{M\Delta f}, \quad \nu_{i,u} = \frac{k_{i,u}}{NT} \quad (2)$$

where $l_{i,u}$ and $k_{i,u}$ are normalized integer delay and Doppler taps. In particular, the values $1/(M\Delta f)$ and $1/(NT)$ are the delay and Doppler resolutions. Equivalently, the DD channel model (1) in matrix form is

$$\mathbf{H}_u = \sum_{i=0}^{L-1} h_{i,u} \mathbf{\Pi}^{l_{i,u}} \mathbf{\Delta}^{k_{i,u}} \quad (3)$$

where $\mathbf{\Pi} \in \mathbb{R}^{MN \times MN}$ is the permutation matrix

$$\mathbf{\Pi} = \begin{bmatrix} 0 & 0 & 0 & \dots & 1 \\ 1 & 0 & 0 & \dots & 0 \\ 0 & 1 & 0 & \dots & 0 \\ \vdots & \vdots & \vdots & \ddots & \vdots \\ 0 & 0 & \dots & 1 & 0 \end{bmatrix} \quad (4)$$

and $\mathbf{\Delta} \in \mathbb{C}^{MN \times MN}$ is a diagonal matrix with the i -th entry $\Delta_i = z^i$, $i \in [MN]$, and $z = \exp(j2\pi/MN)$, see [24].

A. OTFS Modulation Signaling

Consider the multi-user uplink (UL) where each user u transmits an OTFS modulated signal to the AP. The symbols are placed in the DD domain with the matrix $\mathbf{X}_{\text{DD},u} \in \mathbb{C}^{M \times N}$, where $m \in [M]$ and $n \in [N]$ represent the delay and Doppler indices [5]. Applying the inverse symplectic fast Fourier transform (ISFFT), the TF domain matrix is

$$\mathbf{X}_{\text{TF},u}(l,k) = \sum_{n=0}^{N-1} \sum_{m=0}^{M-1} \mathbf{X}_{\text{DD},u}(m,n) e^{j2\pi(\frac{nk}{N} - \frac{ml}{M})}. \quad (5)$$

Following [5], we map the symbols $\mathbf{X}_{\text{TF},u}(l,k)$ to the continuous-time transmitted OTFS signal $s_u(t)$ as

$$\sum_{k=0}^{N-1} \sum_{l=0}^{M-1} \mathbf{X}_{\text{TF},u}(l,k) g_{\text{tx}}(t - kT) e^{j2\pi l \Delta f (t - kT)}, \quad (6)$$

where $\mathbf{X}_{\text{TF},u}(l,k)$ is the (l,k) -th element of the time-frequency domain matrix $\mathbf{X}_{\text{TF},u} \in \mathbb{C}^{M \times N}$ corresponding to the u -th user, and $g_{\text{tx}}(t)$ is the transmit pulse-waveform. We further consider $g_{\text{tx}}(t)$ to be a rectangular pulse.

B. Received Signal Model

The received signal $r(t)$ at the AP is

$$\sum_{u=1}^U \int_{\nu} \int_{\tau} h_u(\tau, \nu) s_u(t - \tau) e^{j2\pi \nu (t - \tau)} d\tau d\nu + w(t). \quad (7)$$

As shown in [5], [24], by sampling at $t = nT/M$ and substituting (2) in (7), the discrete received signal $r(n)$ is

$$\sum_{u=1}^U \sum_{i=0}^{L-1} h_{i,u} e^{j2\pi \frac{k_{i,u}}{MN} ([n - l_{i,u}]_{MN})} s([n - l_{i,u}]_{MN}) + w(n) \quad (8)$$

where $[\cdot]_n$ is the mod- n operation. In the discrete time domain, one can rewrite the sampled received signal as

$$\mathbf{r} = \sum_{u=1}^U \mathbf{H}_u \mathbf{s}_u + \mathbf{w}, \quad (9)$$

where \mathbf{H}_u and \mathbf{s}_u are the time-domain channel matrix (3) and the transmit signal vector for u -th user, respectively. After applying the Wigner transform and performing symplectic fast Fourier transform (SFFT) operation, the end-to-end input-output relation in DD domain is

$$\mathbf{y}_{\text{DD}} = \sum_{u=1}^U \mathbf{H}_{\text{eff},u} \mathbf{x}_{\text{DD},u} + \tilde{\mathbf{w}}_u \quad (10)$$

where $\mathbf{H}_{\text{eff},u} = (\mathbf{F}_N \otimes \mathbf{G}_{\text{rx}}) \mathbf{H}_u (\mathbf{F}_N^H \otimes \mathbf{G}_{\text{tx}})$ is the effective end-to-end DD domain channel matrix corresponding to user u and $\tilde{\mathbf{w}}_u = (\mathbf{F}_N \otimes \mathbf{G}_{\text{rx}}) \mathbf{w}_u$ is the effective noise [24]. The relation (10) can be expressed with a 2D convolution operation shown in (12) below, where the correction factor is

$$\alpha_{i,u}(m,n) = \begin{cases} e^{-j2\pi \frac{m}{N} z^{k_{i,u}([m-l_{i,u}]_M)}} & \text{if } m < l_{i,u} \\ z^{k_{i,u}([m-l_{i,u}]_M)} & \text{if } m \geq l_{i,u} \\ 0 & \text{else.} \end{cases} \quad (11)$$

The correction factor accounts for the phase deviations caused by the loss of bi-orthogonality between the transmitter (Tx) and receiver (Rx) pulses; see [5], [24].

III. OTFS CHANNEL ESTIMATION

A. Compressive Sensing based Channel Estimation

By exploiting sparsity, compressive sensing (CS) permits channel parameter estimation with reduced sampling requirements. We use the OMP algorithm due to its reconstruction accuracy and low computational complexity [25]. We compare the obtained estimation error with that of modified OMP algorithm that considers SCI for the purpose of estimation.

In order to reduce the complexity, we consider the placement of pilot symbols in the time domain by allocating the MN resource vector across multiple users in the uplink.

The (9) can be written as, see Appendix VI,

$$\mathbf{r} = \mathbf{\Psi} \mathbf{h} + \mathbf{n}, \quad (13)$$

where

$$\mathbf{\Psi} = [\mathbf{\Psi}_1, \dots, \mathbf{\Psi}_U], \quad \mathbf{\Psi}_u \in \mathbb{C}^{MN \times l_{\max} k_{\max}} \quad (14)$$

$$\mathbf{h}^T = [\mathbf{h}_1, \dots, \mathbf{h}_U], \quad \mathbf{h}_u \in \mathbb{C}^{l_{\max} k_{\max} \times 1}. \quad (15)$$

The values l_{\max}, k_{\max} are the maximum delay and Doppler shifts; the vectors \mathbf{h}_u and $\mathbf{\Psi}_u$ are the sparse channel coefficient vector and the sensing matrix associated with the u -th user, respectively. The OTFS uplink channel estimation is formulated as a sparse recovery problem as follows:

$$\min \|\mathbf{h}\|_0 \quad \text{s.t.} \quad \mathbf{r} = \mathbf{\Psi} \mathbf{h} + \mathbf{n}. \quad (16)$$

Similar to [21], we use OMP to solve (16), as described in Algorithm 1. In Algorithm 1, the parameters ϵ , \mathbf{S}^n , \mathbf{q} and T^n are the sparsity threshold, the selected support set, the

$$\mathbf{Y}_{\text{DD}}(m, n) = \sum_{u=1}^U \sum_{i=0}^{L-1} h_{i,u} \alpha_{i,u}(m, n) \cdot \mathbf{X}_{\text{DD},u}([m - l_{i,u}]_M, [n - k_{i,u}]_N) + \mathbf{W}_{\text{DD}}(m, n). \quad (12)$$

Input: $\mathbf{r}, \Psi, \epsilon$
Output: $\mathbf{S}^n, \mathbf{h}_{\mathbf{S}^n}$
Initialize: $n = 0, \mathbf{h}^0 = \mathbf{0}, \mathbf{S}^0 = \emptyset, \mathbf{q}^0 = \mathbf{r}$
while ($|\|\mathbf{q}\|_{n-1}^2 - \|\mathbf{q}\|_n^2| > \epsilon$) **do**
 $n = n + 1$
 $T^n = \arg \max |\Psi^H \mathbf{q}^{n-1}|$
 $\mathbf{S}^n = \mathbf{S}^{n-1} \cup T^n$
 $\mathbf{h}_{\mathbf{S}^n} = \Psi_{\mathbf{S}^n}^\dagger \mathbf{r}$
 $\mathbf{q}^{n-1} = \mathbf{q}^n$
 $\mathbf{q}^n = \mathbf{r} - \Psi_{\mathbf{S}^n} \mathbf{h}_{\mathbf{S}^n}$
end

Algorithm 1: OMP Algorithm.

Input: \mathbf{r}, Ψ, L
Output: $\mathbf{S}^n, \mathbf{h}_{\mathbf{S}^n}$
Initialize: $n = 0, \mathbf{h}^0 = \mathbf{0}, \mathbf{S}^0 = \emptyset, \mathbf{q}^0 = \mathbf{r}$
while ($L > 0$) **do**
 $n = n + 1$
 $T^n = \arg \max |\Psi^H \mathbf{q}^{n-1}|$
 $\mathbf{S}^n = \mathbf{S}^{n-1} \cup T^n$
 $\mathbf{h}_{\mathbf{S}^n} = \Psi_{\mathbf{S}^n}^\dagger \mathbf{r}$
 $\mathbf{q}^n = \mathbf{r} - \Psi_{\mathbf{S}^n} \mathbf{h}_{\mathbf{S}^n}$
 $L = L - 1$
end

Algorithm 2: OMP with SCI.

residual vector and the index corresponding to the maximum inner product between the current residual and the adjoint of the sensing matrix, respectively.

If L is known, Algorithm 1 can be modified to Algorithm 2 which has a better computational complexity independent of the threshold; see Sec. IV.

B. Impulse Pilot-based Channel Estimation

Consider impulse pilot-based channel estimation where each user u places an impulse $\delta(l_{p,u}, k_{p,u})$ at location $(l_{p,u}, k_{p,u})$ in the DD domain of size $M \times N$, where $l_{p,u}$ and $k_{p,u}$ are the delay and Doppler indices. The location of the pilot x_p of user u is

$$\mathbf{X}_{\text{DD},u}(l, k) = \begin{cases} x_p & \text{if } l = l_{p,u}, k = k_{p,u} \\ 0 & \text{else.} \end{cases} \quad (17)$$

Let l_{\max} and k_{\max} be the maximum spreads on the delay and Doppler axes from the pilot's location, respectively. Considering all the users' pilots are with sufficient guard band, the channel estimation can be performed without multi-user interference; see (12). In particular, the threshold-based channel estimation \hat{h}_i of the i -th path at location (l_i, k_i) is

$$\hat{h}_i = \frac{\mathbf{Y}_{\text{DD}}(l_i, k_i)}{x_p \alpha_i(l_i, k_i)} \quad \text{if } \mathbf{Y}_{\text{DD}}(l_i, k_i) > \tau, \quad (18)$$

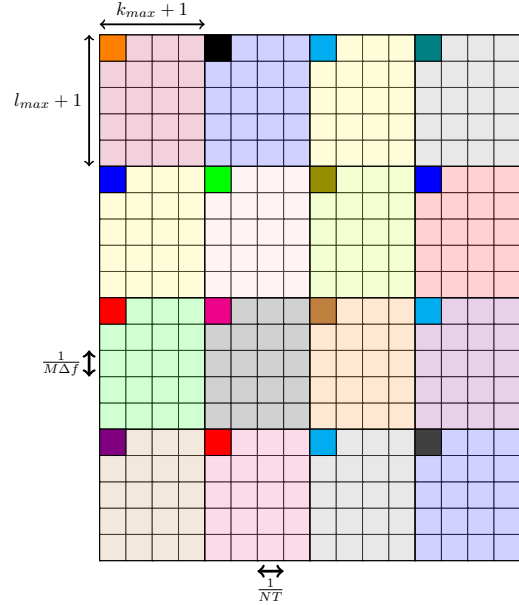


Fig. 1. DD grid with maximum possible pilot symbols with associated guard bands.

for some threshold τ .

The overall number of pilot and guard symbols needed for perfect channel estimation at the AP is $(l_{\max} + 1)(k_{\max} + 1)$ per user. Thus, for an $M \times N$ grid, the maximum number of users that can be estimated simultaneously and independently is $\lfloor MN / (l_{\max} + 1)(k_{\max} + 1) \rfloor$; Fig. (1).

C. Embedded Data Transmission and Channel Estimation

The estimation method in Sec. III-B uses the entire grid for channel estimation which reduces spectral efficiency in general. Instead, when serving a small number of users, one may fill the empty DD grid with information symbols to improve spectral efficiency. We propose a strategic data placement alongside the pilots to increase spectral efficiency.

Consider a pilot symbol located at $(0,0)$ of the DD grid and assume l_{\max} and k_{\max} are the maximum delay and Doppler shifts; see Fig. 1. We need a guard band at all corners to avoid data collisions, in addition to the guard band of size $(l_{\max} + 1)(k_{\max} + 1)$ in the upper left corner. This gives a total guard band of size $4l_{\max}k_{\max} + 2l_{\max} + 2k_{\max} + 1$.

By adding a second user's pilot below the first user's guard band, see Fig. 3, we need an additional guard band with $2l_{\max}k_{\max} + l_{\max} + 2k_{\max} + 1$ symbols. The reduction is due to the presence of the guard band associated with the first user. Similarly, by adding a third user, we need an additional guard band with $2l_{\max}k_{\max} + 2l_{\max} + k_{\max} + 1$ symbols. Finally, the fourth user's pilot can be added with an additional guard

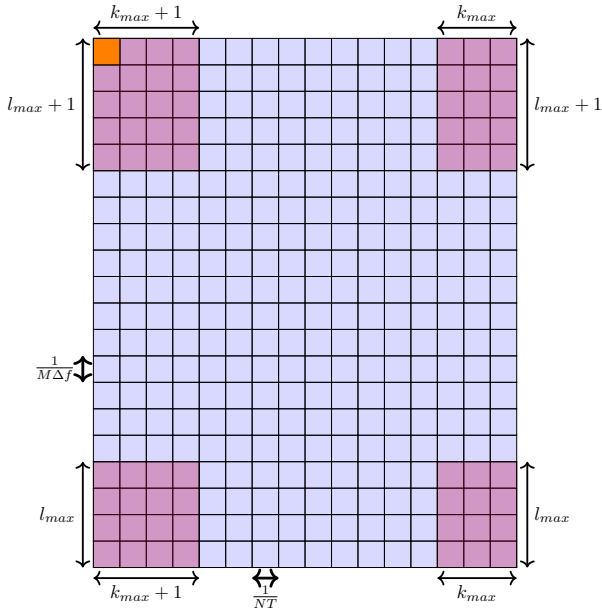


Fig. 2. DD grid with pilot and data for a single user.

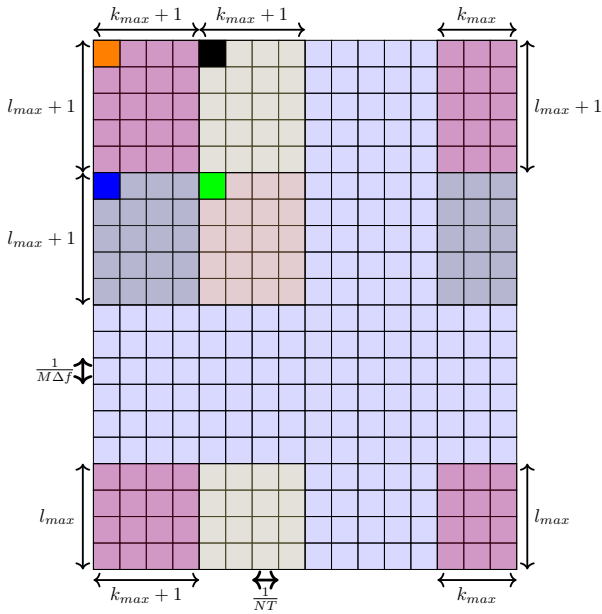


Fig. 3. DD grid with pilot and data for four users.

band of $l_{\max}k_{\max} + l_{\max} + k_{\max} + 1$ symbols. This process can be continued until all user's pilots are placed; see Fig. 3.

After channel estimation, the receivers perform multi-user detection by extending the linear estimation technique mentioned in [26]. We rewrite (10) as

$$\mathbf{y}_{\text{DD}} = \mathbf{H}'_{\text{eff}} \tilde{\mathbf{x}}_{\text{DD}} + \mathbf{n} \quad (19)$$

where

$$\mathbf{H}'_{\text{eff}} = [\mathbf{H}_{\text{eff},1}, \dots, \mathbf{H}_{\text{eff},U}], \quad \mathbf{H}_{\text{eff},u} \in \mathbb{C}^{MN \times MN} \quad (20)$$

$$\tilde{\mathbf{x}}_{\text{DD}}^{\text{T}} = [\mathbf{x}_{\text{DD},1}, \dots, \mathbf{x}_{\text{DD},U}], \quad \mathbf{x}_{\text{DD},u} \in \mathbb{C}^{MN \times 1}. \quad (21)$$

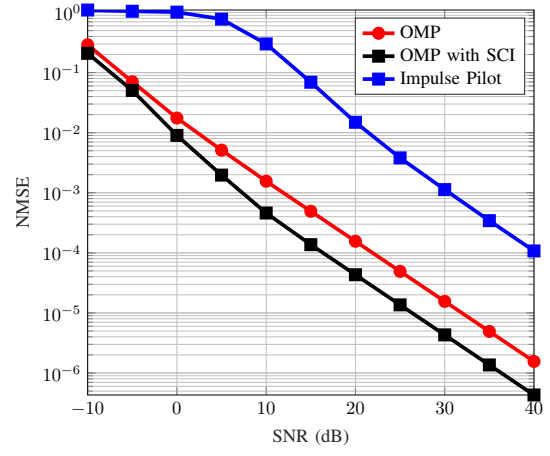


Fig. 4. NMSE comparison for four users.

If the AP knows the users' pilot locations, it can eliminate the effect of the pilot symbol from (19) and compute

$$\mathbf{y}_{\text{DD},\mathcal{D}} = \mathbf{y}_{\text{DD}} - x_p \mathbf{H}'_{\text{eff}}(:, \mathcal{P}), \quad (22)$$

where \mathcal{D} and \mathcal{P} are the set of indices related to the data symbols and pilot symbols in $\tilde{\mathbf{x}}_{\text{DD}}$ respectively. After threshold-based channel estimation, the sub-matrix corresponding to data indices for the estimated channel matrix \mathbf{H}'_{eff} can be computed as

$$\hat{\mathbf{H}}'_{\text{eff},\mathcal{D}} = \hat{\mathbf{H}}'_{\text{eff}}(:, \mathcal{D}). \quad (23)$$

The resulting input-output model for the system is

$$\mathbf{y}_{\text{DD},\mathcal{D}} = \hat{\mathbf{H}}'_{\text{eff},\mathcal{D}} \mathbf{x}_{\text{DD},\mathcal{D}} + \mathbf{n}, \quad (24)$$

and detection can be accomplished by an linear minimum mean square error (LMMSE) estimator to output

$$\hat{\mathbf{x}}_{\text{DD},\mathcal{D}}^{\text{MMSE}} = (\hat{\mathbf{H}}'_{\text{eff},\mathcal{D}}{}^{\text{H}} \hat{\mathbf{H}}'_{\text{eff},\mathcal{D}} + \frac{1}{\text{SNR}} \mathbf{I})^{-1} \hat{\mathbf{H}}'_{\text{eff},\mathcal{D}}{}^{\text{H}} \mathbf{y}_{\text{DD},\mathcal{D}}. \quad (25)$$

IV. NUMERICAL RESULTS

We simulate with a DD grid with $M \times N = 32 \times 32$ bins and the carrier frequency $f_c = 4$ GHz with a sub-carrier spacing of $\Delta f = 15$ kHz. binary phase-shift keying (BPSK) modulation was used for the pilot symbols and we consider $L = 4$ independent and identically distributed (i.i.d.) paths with a random power-delay profile. This model includes scatterers in the communication environment, adding a layer of realism. We investigate the robustness of the above CS-based and impulse-based channel estimation algorithms.

Fig. 4 and Fig. 5 show the normalized mean square error (NMSE) vs. the pilot symbol signal-to-noise ratio (SNR) with four and six users respectively. Fig. 4 shows that OMP outperforms impulse pilot-based estimation. However, Fig. 5 shows that if one increases the number of users, OMP performs worse than impulse pilot-based estimation. The reason being the reduced number of pilot symbols for the channel estimation purpose. Since the sensing matrix absorbs the pilot vectors and is used for the purpose of sparse vector estimation, the lack of enough pilot symbols results in performance degradation. In

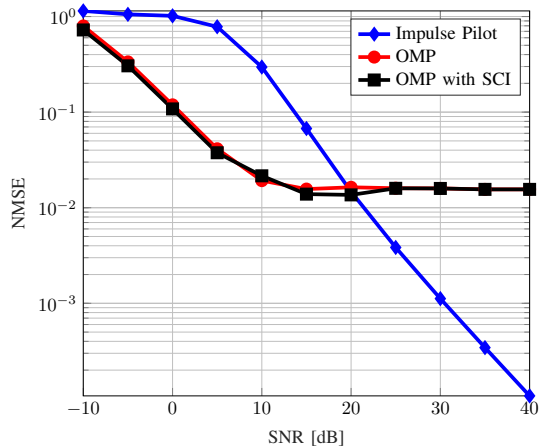


Fig. 5. NMSE comparison for six users.

order to maintain the performance the number of pilots used must be increased in turn leading to an increase in the size of M and N . On the other hand, the impulse pilot-based approach is independent of the number of users, as it is possible to notice that the curve is the same in Fig. 4 and Fig. 5. Further, we also capture the variation in the estimation using OMP for different threshold values. In Fig. 4, we can observe that by choosing a right threshold value we can improve the estimation accuracy close to that of OMP-SCI.

The computational complexity of OMP-SCI in terms of operation time and number of iterations is smaller than OMP by aligning the number of iterations with the effective number of channel taps. In general, OMP-SCI needs less than half the operating time and a much smaller number of least-squares (LS) operations compared to conventional OMP. For instance, considering the scenario with four users and a fixed number of simulation cycles, it is observed that the OMP takes approximately 45 s to complete the estimation process, while the OMP-SCI takes approximately 22 s. Straightforwardly, it is calculated that, for the same scenario, the OMP implies up to 35983 operations for the estimation, while the OMP-SCI reduces this number to approximately 26400 operations.

Though the estimation process efficiency of the impulse pilot-based method is not affected by the number of users, it is affected by the threshold power level used for detecting the channel tap. Fig. 6 shows that the estimation error depends on the threshold.

Fig. 7 plots the bit error rate (BER) of embedded impulse pilot-based channel estimation and data detection with the proposed pilot placement. We consider four users as in Fig. 3 and use quadrature phase-shift keying (QPSK) modulation for the data symbols. A LMMSE decoder is used and the results are compared to having full channel knowledge. Fig. 7 shows the perfect and imperfect CSI curves almost match, which demonstrates the proposed approach is reliable, especially at low SNR. There is a BER degradation which depends on the number of users, but it is less severe for more than three users.

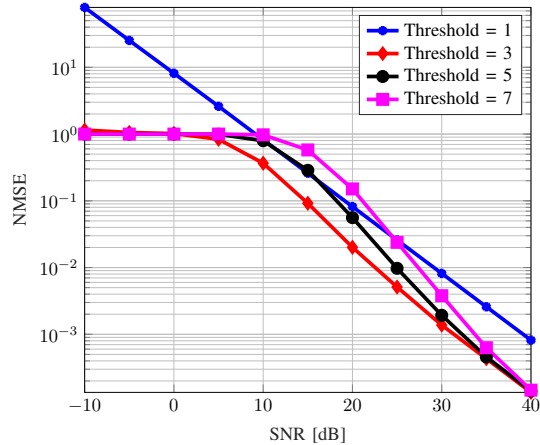


Fig. 6. NMSE comparison for different values of threshold τ in impulse pilot based estimation.

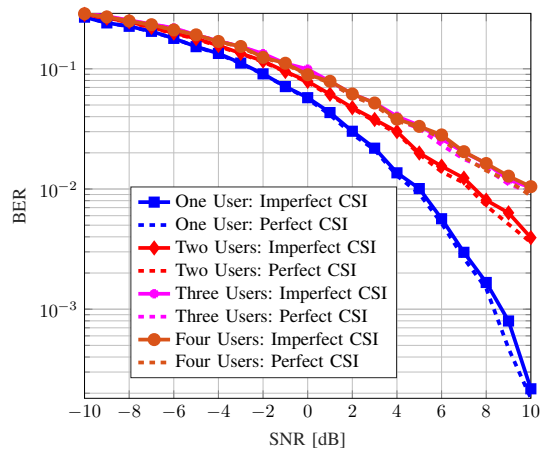


Fig. 7. BER comparison in a different number of user scenarios.

V. CONCLUSIONS

We compared channel estimation algorithms for OTFS for multi-user scenarios. An impulse pilot-based allocation method decreases the estimation of computational complexity. Numerical results show that the choice of estimation algorithm should depend on the number of users. For instance, for a small number of users, OMP outperforms the impulse-pilots, while for a large number of users, impulse-pilots are better. The proposed algorithms have lower complexities than conventional OMP.

ACKNOWLEDGMENT

The authors would like to thank Prof. Gerhard Kramer for constructive feedback.

The research of Lorenzo Zaniboni is funded by Deutsche Forschungsgemeinschaft (DFG) through the grant KR 3517/12-1.

VI. APPENDIX

Without loss of generality, we derive the model considering two users. Consider $\mathbf{s}_1 \in \mathbb{C}^{MN}$ and $\mathbf{s}_2 \in \mathbb{C}^{MN}$ be time

domain sequences corresponding to user 1 and user 2 respectively. Note that the sequence contains pilot symbols placed in an orthogonal fashion. For example, we can consider \mathbf{s}_1 to have pilot symbols from index 0 to $\frac{MN}{2} - 1$ and \mathbf{s}_2 to have pilot symbols placed from index $\frac{MN}{2}$ to $MN - 1$.

At the AP, the received signal can be given as

$$r(t) = \sum_{u=1}^2 r_u(t) = \sum_{u=1}^2 \sum_{i=0}^{L-1} h_{i,u} s(t - \tau_{i,u}) e^{j2\pi\nu_{i,u}(t - \tau_{i,u})} + w(t). \quad (26)$$

Note that without loss of generality, we consider the number of multi-path components for the users to be the same. Now, sampling the received signal with a sampling time interval of $\frac{T}{M}$, we can rewrite the received signal in the discrete-time domain as

$$\mathbf{r} = \sum_{u=1}^2 \sum_{l_u=0}^{l_{max}-1} \sum_{k_u=0}^{k_{max}-1} (h_{l_u, k_u} \mathbf{\Pi}^{l_u} \mathbf{\Delta}^{k_u}) \mathbf{s}_u + \mathbf{w}. \quad (27)$$

Let us represent the product of the matrices $\mathbf{\Pi}^{l_u} \mathbf{\Delta}^{k_u} \mathbf{s}_u = \mathbf{\Psi}_{l_u, k_u}$, we can rewrite the expression as

$$\mathbf{r} = \sum_{u=1}^2 \sum_{l_u=0}^{l_{max}-1} \sum_{k_u=0}^{k_{max}-1} h_{l_u, k_u} \mathbf{\Psi}_{l_u, k_u} + \mathbf{w}. \quad (28)$$

$$\begin{aligned} \mathbf{r} &= [\mathbf{\Psi}_1 \quad \mathbf{\Psi}_2] \begin{bmatrix} \mathbf{h}_1 \\ \mathbf{h}_2 \end{bmatrix} + \mathbf{n} \\ &= \mathbf{\Psi} \mathbf{h} + \mathbf{n}. \end{aligned} \quad (29)$$

REFERENCES

- [1] E. Biglieri, R. Calderbank, A. Constantinides, A. Goldsmith, A. Paulraj, and H. V. Poor, *MIMO wireless communications*. Cambridge university press, 2007.
- [2] H. Q. Ngo, A. Ashikhmin, H. Yang, E. G. Larsson, and T. L. Marzetta, "Cell-free massive MIMO: Uniformly great service for everyone," in *IEEE Int. Workshop Signal Proc. Advances wireless Commun.* IEEE, 2015, pp. 201–205.
- [3] Ö. T. Demir, E. Björnson, L. Sanguinetti *et al.*, "Foundations of user-centric cell-free massive MIMO," *Foundations and Trends® in Signal Processing*, vol. 14, no. 3-4, pp. 162–472, 2021.
- [4] R. Hadani and A. Monk, "OTFS: A new generation of modulation addressing the challenges of 5g," *arXiv preprint arXiv:1802.02623*, 2018.
- [5] R. Hadani, S. Rakib, M. Tsatsanis, A. Monk, A. J. Goldsmith, A. F. Molisch, and R. Calderbank, "Orthogonal time frequency space modulation," in *IEEE Wireless Commun. and Network. Conf.* IEEE, 2017, pp. 1–6.
- [6] L. M. W. Lopez and M. Bengtsson, "Achievable rates of orthogonal time frequency space (otfs) modulation in high speed railway environments," in *IEEE Annual Int. Symp. Personal, Indoor and Mobile Radio Commun. (PIMRC)*. IEEE, 2022, pp. 982–987.
- [7] C. An and H.-G. Ryu, "High throughput mobile communication based on otfs system with the delay-doppler compensation," *Wireless Personal Commun.*, vol. 106, pp. 473–486, 2019.
- [8] P. Raviteja, E. Viterbo, and Y. Hong, "OTFS performance on static multipath channels," *IEEE Wireless Commun. Letters*, vol. 8, no. 3, pp. 745–748, 2019.
- [9] A. Mohammadi, S. Chakkor, A. El Oualkadi, M. Moussaoui, A. Dkiouak, and M. Baghour, "Performance Evaluation of OTFS and OFDM for 6G Waveform," in *ITM Web of Conf.s*, vol. 48. EDP Sciences, 2022, p. 01015.
- [10] L. Gaudio, G. Colavolpe, and G. Caire, "OTFS vs. OFDM in the presence of sparsity: A fair comparison," *IEEE Trans. Wireless Commun.*, vol. 21, no. 6, pp. 4410–4423, 2021.
- [11] F. Lampel, A. Avarado, and F. M. Willems, "On OTFS using the discrete Zak transform," in *IEEE Int. Conf. on Commun. Workshops*. IEEE, 2022, pp. 729–734.
- [12] S. K. Mohammed, R. Hadani, A. Chockalingam, and R. Calderbank, "OTFS—a Mathematical Foundation for Communication and Radar Sensing in the Delay-Doppler Domain," *IEEE BITS Inf. Theory Mag.*, vol. 2, no. 2, pp. 36–55, 2022.
- [13] M. Guo and M. C. Gursoy, "Joint activity detection and channel estimation in cell-free massive mimo networks with massive connectivity," *IEEE Trans. Commun.*, vol. 70, no. 1, p. 317–331, Jan. 2022. [Online]. Available: <http://dx.doi.org/10.1109/TCOMM.2021.3122471>
- [14] H. Song, T. Goldstein, X. You, C. Zhang, O. Tirkkonen, and C. Studer, "Joint channel estimation and data detection in cell-free massive mimo systems," 2021.
- [15] K. R. Murali and A. Chockalingam, "On otfs modulation for high-doppler fading channels," in *Inf. Theory Appl. Workshop*. IEEE, 2018, pp. 1–10.
- [16] M. K. Ramachandran and A. Chockalingam, "Mimo-otfs in high-doppler fading channels: Signal detection and channel estimation," in *IEEE Global Commun. Conf.* IEEE, 2018, pp. 206–212.
- [17] G. D. Surabhi, R. M. Augustine, and A. Chockalingam, "Multiple access in the delay-doppler domain using otfs modulation," 2019.
- [18] Z. Wei, W. Yuan, S. Li, J. Yuan, and D. W. K. Ng, "Off-grid channel estimation with sparse bayesian learning for otfs systems," *IEEE Trans. Wireless Commun.*, vol. 21, no. 9, pp. 7407–7426, 2022.
- [19] S. Srivastava, R. K. Singh, A. K. Jagannatham, and L. Hanzo, "Bayesian learning aided simultaneous row and group sparse channel estimation in orthogonal time frequency space modulated mimo systems," *IEEE Trans. Commun.*, vol. 70, no. 1, pp. 635–648, 2021.
- [20] L. Li, Y. Liang, P. Fan, and Y. Guan, "Low complexity detection algorithms for otfs under rapidly time-varying channel," in *IEEE Vehic. Technol. Conf. (VTC2019-Spring)*. IEEE, 2019, pp. 1–5.
- [21] O. K. Rasheed, G. Surabhi, and A. Chockalingam, "Sparse delay-doppler channel estimation in rapidly time-varying channels for multiuser otfs on the uplink," in *IEEE Vehic. Technol. Conf. (VTC2020-Spring)*. IEEE, 2020, pp. 1–5.
- [22] P. Raviteja, K. T. Phan, and Y. Hong, "Embedded pilot-aided channel estimation for otfs in delay-doppler channels," *IEEE Trans. vehic. Technol.*, vol. 68, no. 5, pp. 4906–4917, 2019.
- [23] H. B. Mishra, P. Singh, A. K. Prasad, and R. Budhiraja, "Otf channel estimation and data detection designs with superimposed pilots," *IEEE Trans. wireless Commun.*, vol. 21, no. 4, pp. 2258–2274, 2021.
- [24] P. Raviteja, Y. Hong, E. Viterbo, and E. Biglieri, "Practical pulse-shaping waveforms for reduced-cyclic-prefix otfs," *IEEE Trans. Vehic. Technol.*, vol. 68, no. 1, pp. 957–961, 2018.
- [25] A. Draganic, I. Orovic, and S. Stankovic, "On some common compressive sensing recovery algorithms and applications-review paper," *arXiv preprint arXiv:1705.05216*, 2017.
- [26] A. Mehrotra, R. K. Singh, S. Srivastava, and A. K. Jagannatham, "Channel Estimation Techniques for CP-Aided OTFS Systems Relying on Practical Pulse Shapes," in *IEEE Int. Conf. Signal Proc. Commun.* IEEE, 2022, pp. 1–5.